Proceedings of the 2018 IEEE
International Conference on Robotics and Biomimetics
December 12-15, 2018, Kuala Lumpur, Malaysia

Design and Validation of Multi-Layer Brakes for a Lockable Stand for a Surgical Robotic System*

Tianlai Dong, Yuyang Chen, Lingyun Zeng, Zenghui Liu and Kai Xu, *Member, IEEE*

***Abstract*—MPL (multi-port laparoscopy) has mostly replaced traditional open surgery due to several advantages, such as less postoperative complications and faster recovery. However, manual manipulation of the laparoscopic surgical tools can be challenging and exhausting. Numerous robotic systems were hence developed to assist surgeons. A majority of the existing developments followed a similar approach that a manipulator maneuvers a stick-like surgical tool for intra-abdominal surgical tasks. The surgical tool is usually equipped with a wrist for distal dexterity, while the manipulator is required to realize RCM (Remote Center of Motion) movements in order to prevent the surgical tool from tearing a patient's abdominal wall. However, a continuum surgical manipulator with 6 DoFs (Degrees of Freedom) can provide sufficient mobility for intra-abdominal movements. Therefore, only a lockable stand that holds such a continuum surgical manipulator, instead of an RCM mechanism, is needed during a procedure. Compact and reliable joint brakes with high locking torques and rapid actuation are needed for such a lockable stand. Inspired by the layered jamming principle, this paper presents the design, construction and verification of multi-layer brakes for the lockable stand. The experimental validation of the multi-layer brakes is elaborated to demonstrate the functionality and the effectiveness of the proposed idea.**

I. Introduction

MPL (multi-port laparoscopy) has considerable advantages comparing to traditional open surgery, such as less pain and hemorrhage, reduced postoperative complications, and shorter recovery time [1]. Although MPL is beneficial, manual manipulation of the laparoscopic surgical tools can be challenging and exhausting due to insufficient distal dexterity and inverted tool-maneuvering movements. Numerous robotic systems were hence developed to assist surgeons in MPL [2-4].

A majority of the existing developments followed a similar approach that a manipulator maneuvers a stick-like surgical tool for intra-abdominal surgical tasks [3, 5-9]. The surgical tool is usually equipped with a wrist for enhanced distal dexterity, while the manipulator is required to realize RCM (Remote Center of Motion) movements in order to prevent the surgical tool from tearing a patient's abdominal wall [10, 11].

*This work was supported in part by the National Natural Science Foundation of China (Grant No. 51722507, Grant No. 51435010 and Grant No. 91648103), and in part by the National Key R&D Program of China (Grant No. 2017YFC0110800).

Tianlai Dong, Yuyang Chen and Zenghui Liu are with the RII Lab (Lab of Robotics Innovation and Intervention), UM-SJTU Joint Institute, Shanghai Jiao Tong University, Shanghai, China (emails: 5123709073@sjtu.edu.cn, supandoria@sjtu.edu.cn and liuzenghui@sjtu.edu.cn).

Lingyun Zeng and Kai Xu are with the School of Mechanical Engineering, Shanghai Jiao Tong University, Shanghai, China (emails: me_maxqi@sjtu.edu.cn and k.xu@sjtu.edu.cn, corresponding author: K. Xu).

On the other hand, a continuum surgical manipulator with 6 distal DoFs (Degrees of Freedom) can provide sufficient mobility for intra-abdominal movement [12-14]. While using such a continuum surgical manipulator, a RCM mechanism is no longer needed to mobilize the base of the continuum surgical manipulator during operations. Instead, a lockable stand holding the continuum surgical manipulator during surgery is required.

The lockable stand for holding the continuum surgical manipulator in a surgical robotic system is hence designed as in Fig. 1, with 4 revolute joints and 1 prismatic joint, in order to position and orient the continuum surgical manipulator with enough mobility. Locking of the revolute joints should be reliable, even under the disturbances exerted on the continuum surgical manipulator during surgery. Actuation of the locking and releasing movements should be rapid such that the lockable stand can be safely and conveniently adjusted in preoperative preparations [4].

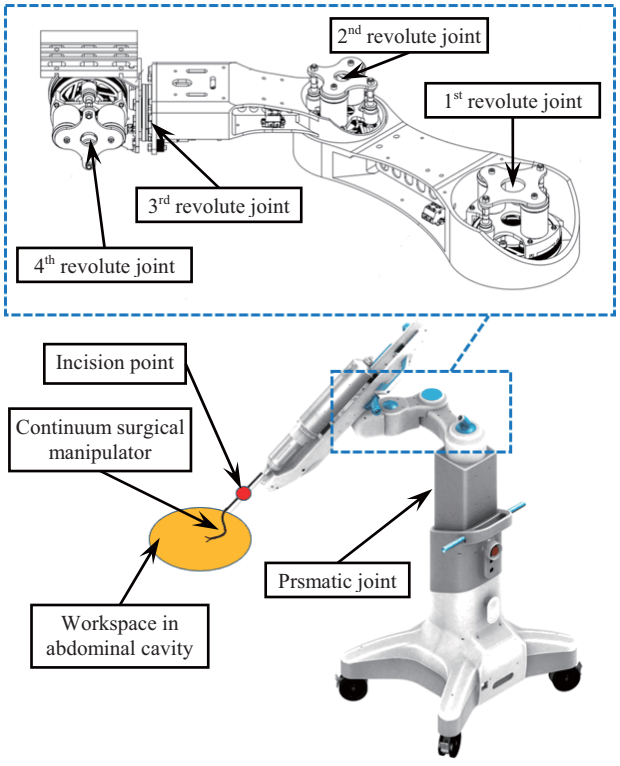

Figure 1. The lockable stand in a surgical robotic system

The revolute joint brakes needed for this lockable stand are not commercially available. The existing products either have insufficient locking torques or are too bulky and heavy [15, 16].

978-1-7281-0377-8/18/$31.00 © 2018 IEEE

Inspired by the layered jamming principle that the friction between two sliding components can be amplified by using an interwoven multiple thin-layer structure [17, 18], this study aims at designing compact and light-weighted joint brakes with large locking torques and rapid actuation, for the four revolute joints of the lockable stand in Fig. 1. As the joint brakes shall satisfy different application conditions for the four revolute joints, three types of the joints brakes (the large, the medium and small ones) are designed.

The rest of this paper is organized as follows. Section II presents the design objectives and design overview. Design descriptions and calculations for the components of the multi-layer brakes are presented in Section III. A preliminary experimentation for verifying the locking capacity and lifespan of the multi-layer brakes is reported in Section IV. Conclusions and future works are summarized in Section V.

II. Design Objectives and Overview

Aiming at meeting the operational requirements for the lockable stand of a surgical robotic system, three types of the multi-layer brakes (the large, the medium and small ones) are designed: the large brake for the first joint, the medium brake for the second joint, and the small brake for the third and fourth revolute joints. Then the design objectives of the joint brakes are listed as follows.

- The multi-layer brakes should be compact to minimize the size of the lockable stand. The outer diameters of the large, medium and small multi-layer brakes are constrained to 120 mm, 100 mm and 80 mm, respectively.
- The large, medium and small multi-layer brakes should possess a rated locking capacity of 90 Nm, 70 Nm and 40 Nm, respectively. While locked, the angular output should not exceed 0.5° if the rated loading torque is exerted.
- While released, the rotary friction should not exceed 1% of the rated locking capacity. In this way, the reposition and re-orientation of the lockable stand in the preoperative preparations can be carried out smoothly. This feature improves the usability of the surgical stand.
- The locking and releasing actuation for the multi-layer brakes should be reliable and rapid to ensure the safety and usability.
- The multi-layer brake should have a standalone modular design such that the assembling can be convenient.

The multi-layer brakes are hence designed to achieve the aforementioned design objectives with the medium one shown in Fig. 2. The brake mainly consists of i) a cross-roller bearing, ii) a multi-layer structure, and iii) a pressing assembly.

Using the medium brake in Fig. 2 as an example, the entire brake sits on a cross-roller bearing such that the brake becomes a standalone module. The cross-roller bearing is an ideal option since it is widely used in robotic arms due to its high load-bearing capacity and structural rigidity. Parts that rotate with respect to each other can be conveniently mounted to the bottom surface of the cross-roller bearing of the brake. The outer diameters of these cross-roller bearings for the large, medium and small joint brakes are 120 mm, 95 mm and 70 mm, respectively.

The multi-layer structure is shown in the inset of Fig. 2 and Fig. 3. While pressed by the pressing assembly, a high frictional locking torque is expected to be generated due to the layered jamming principle.

Two electromagnets are used in the pressing assembly for the brake actuation in Fig. 2. The electromagnets are selected primarily due to their rapid actuation. The attraction forces generated by the electromagnets will press the multi-layer structure via two steel rods guided by two linear bearings.

The presented design in Fig. 2 might seem similar to that in [19] where multiple brake disks were used. Two major differences should be noted. First, thin stainless steel disks are used in the proposed multi-layer structure. They are pressed to deform to become contacted to generate friction. While released, the thin stainless steel disks will restore to their non-contacting status. Hence the frictional torque of the brake is particularly small if the brake is released. Second, electromagnets, instead of the ball screws powered by motors, are used in the proposed design. The actuation response is quicker and the cost can be lower.

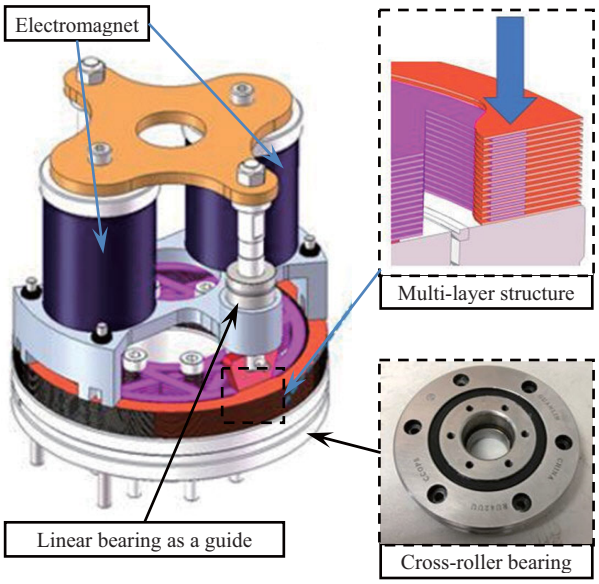

Figure 2. Design overview of the multi-layer brake

III. Design Descriptions

The multi-layer brake has two major components: the multi-layer structure and the pressing assembly. These two components are described in detail in this section, using the design of the medium brake as an example.

A. Multi-Layer Structure

The multi-layer structure consists of a stack of disks, including i) the stator friction disks, ii) the stator spacers, iii) the rotor friction disks, and iv) the rotor spacers. All the disks are arranged in an alternating sequence and assembled onto the cross-roller bearing as shown in Fig. 3.

The stator friction disks and the stator spacers are assembled alternatingly onto the outer ring of the cross-roller bearing, while the rotor friction disks and the rotor spacers are assembled alternatingly onto the inner ring. The overlap between the stator friction disks and the rotor friction disks is the pressing area to be pressed by the pressing assembly.

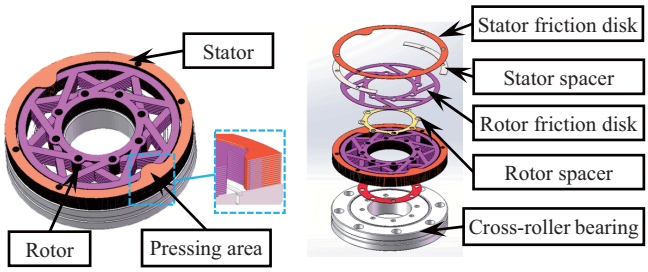

Figure 3. Design of the multi-layer structure

All the disks were made from stainless steel thin sheets via laser cutting. As shown in Fig. 4, when the multi-layer brake is released, the stator friction disks and the rotor friction disks were not in contact. This (very small) distance between the stator friction disk and the rotor friction disk leads to small friction torque of the brake under this released status.

When the multi-layer brake is actuated, the disks are pressed to deform to close all the gaps between the disks. Friction would be generated from these disks that are squeezed together. The total deformation should be smaller than the stroke of the electromagnet actuation, limiting the number of friction disks deployed in the multi-layer brake.

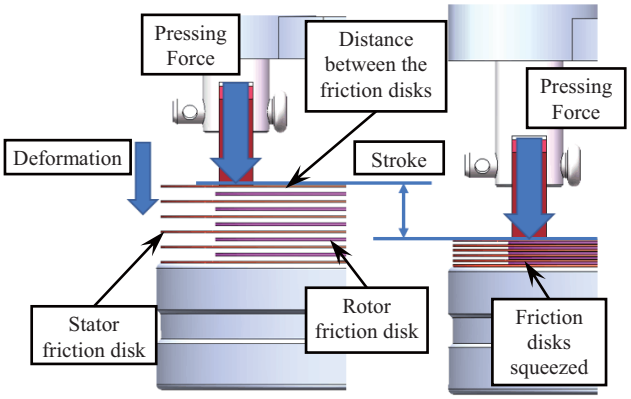

Figure 4. Actuation process of the multi-layer brake

Furthermore, the rotor friction disks and the stator friction disks are squeezed together to generate amplified friction, while the brake is actuated. However, a part of the pressing force will be used to deform the friction disks along the pressing direction. Hence, a low rigidity along the pressing direction at the pressing area is preferred. The profiles of the friction disks shall be specifically designed, as shown in Fig. 5.

The profile of the stator friction disk is designed as in Fig. 5(a). Referring to Fig. 3, when the stator spacers and the stator friction disks are alternatingly arranged and fixed to the outer ring of the cross-roller bearing, the two quarters become fixed. When the pressing area is pressed to squeeze the friction disks, the two deformable quarters of the stator friction disk act as beams fixed at both ends, contributing to a low stiffness along the pressing direction, as preferred.

The profile of the rotor friction disk is designed as in Fig. 5(b), consisting of an inner ring, an outer ring and several spokes in the tangential directions. The pressing area is over the outer ring. The spokes in the tangential directions lead to extended lengths such that the spokes will deform more easily along the pressing direction. The outer ring should have a diameter as large as possible to generate a large moment arm for the locking torque.

The locking torque is essentially generated by the forces along the spokes between the inner rings and the outer rings of the rotor friction disks, since the inner rings of the rotor friction disks are all fixed to the inner rings of the cross-roller bearing. The spokes in the tangential directions help increase the torque generating capacities. What's more, in order to generate a balanced performance of locking the joint in both directions, the rotor friction disks are arranged alternatingly (one face up and one face down), as shown in Fig. 3.

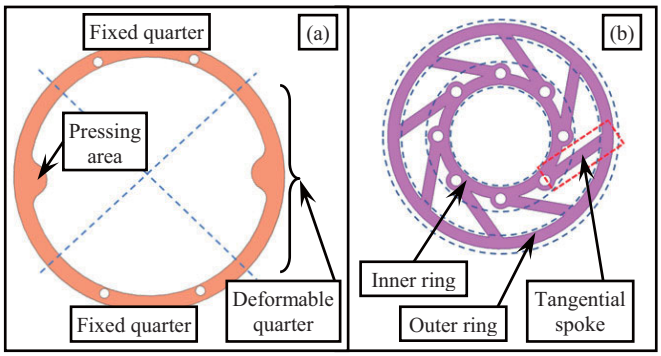

Figure 5. Profile design of the disks: (a) the stator friction disk, and (b) the rotor friction disk

B. *Pressing Assembly*

The pressing assembly transmits the attraction force between the permanent electromagnet and the iron block to the pressing force exerted on the pressing area as shown in Fig.6.

The permanent electromagnet is selected for safety considerations. The attraction force between the iron block and the permanent magnet is maintained when the power is off [16]. Then the brake stays in a locked status. When the power is on, the magnet field is neutralized and the attraction force is diminished. The brake is then in a released status.

In order to maximize the utilization of the design volume, two electromagnets are arranged in the medium-sized brake as shown in Fig. 6. The two electromagnets are fixed symmetrically to a mounting base that is connected to the stator. Two iron blocks are fixed to a mounting plate that is connected to a pair of steel rods. The steel rods are guided by two linear bearings. An adaptive pressing block is used at one end of each steel rod to exert a uniformly distributed pressing force onto the pressing area, in order to prevent stress concentration and reduce overall wear.

The attraction force between the electromagnet and the iron block decays exponentially as the gap between them increases.

Hence a particular advantage of this design is that the attraction force becomes larger when the steel rods press the friction disks harder. When the distance between the electromagnet and the iron block approaches zero, a maximal pressing force is reached.

According to the specification of the electromagnet, the maximum attraction force is 210 N when the gap is zero. The attraction force is only 6 N when the gap increases to 0.8 mm.

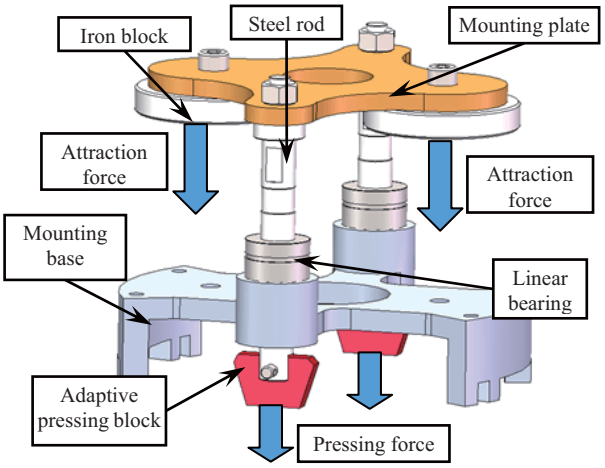

Figure 6. Design of the pressing assembly

C. Design Calculations for the Multi-Layer Brake

The locking capacity for the multi-layer brake can be estimated in (1).

$$T = 2nkF\mu_s r_{eqv} \tag{1}$$

Where, n is the number of rotor friction disks, the number of the contact areas is $2n$ because each rotor friction disk has two faces; k is the number of electromagnets deployed in a multi-layer brake which is limited by the available space; F is the maximum attraction force between the electromagnet and the iron block when the gap between them is zero; r_{eqv} is the distance between the brake center and the equivalent pressing spot of the pressing area, which can be approximated as in (2).

$$r_{eqv} = \frac{1}{2}\left(r_{out1} + r_{out2}\right) \tag{2}$$

Where r_{out1} and r_{out2} is the inner and outer radii of the outer ring of the rotor friction disk, respectively.

Taking the calculation for the medium multi-layer brake as an example, two electromagnets are used, which leads to $k = 2$. The inner and outer radii of the outer ring of the rotor friction disk are $r_{out1} = 41.5$ mm and $r_{out2} = 47$ mm, respectively. Then $r_{eqv} = 44.25$ mm. The target locking capacity is $T = 70$ Nm. The minimal number of the rotor friction disks is in (3), using a friction coefficient between a steel-steel contact of $\mu_s = 0.13$.

$$n_{\min} = \frac{T}{2 \cdot k \cdot F \cdot \mu_s \cdot r_{eqv}} = 14.5 \tag{3}$$

Due to the availability of the stainless steel sheets in stock, the thicknesses of the rotor friction disk, the rotor spacer, the stator friction disk and the stator spacer are selected at 0.30 mm, 0.30 mm, 0.25 mm, and 0.35 mm, respectively. Since the stator spacer disk is 0.05 mm thicker than the rotor friction disk, the distance between the rotor friction disk and the stator friction disk is 0.025 mm. The total squeezing distance s = n×2×0.025 mm should be smaller than the effective attraction distance of 0.8mm. Hence n should be less than 16. Then, n = 15 is adopted.

Considering the aforementioned design objectives and following the same design approach, the large and the small multi-layer brakes for the revolute joints in the lockable stand can be obtained as shown in Table I. and Fig. 7.

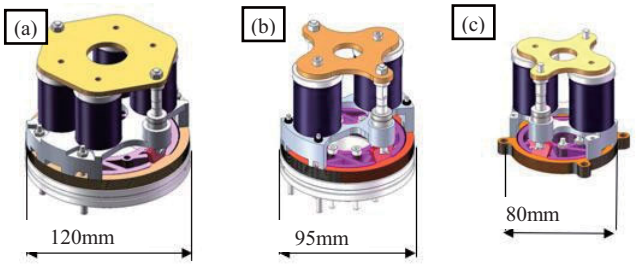

Figure 7. Designs of the (a) large, (b) medium, and (c) small multi-layer brakes for the lockable stand

TABLE I. DESIGN RESULTS OF THE JOINT BRAKES

Design Outputs	Multi-layer brakes		
	Large	***Medium***	***Small***
Outer diameter (mm)	120	95	70
Numbers of the arranged electromagnets (pieces)	4	2	2
Numbers of the rotor friction disks (pieces)	15	15	15
Stroke (mm)	0.75	0.75	0.75
Applied in the lockable stand	Joint 1	Joint 2	Joint 3&4

IV. PRELIMINARY EXPERIMENTATION

To verify the functionality for the presented multi-layer brakes, preliminary experimentation was carried out. The locking capacity, the released rotary friction and the lifespan are tested using a customized test rig as shown in Fig. 8.

In the test rig in Fig. 8, the multi-layer brake to be tested is fixed to the bench with the outer ring of the cross-roller bearing connected to an L-shaped fixture. A torque motor was used to exert an adjustable torque on the shaft that is connected with the inner ring of the cross-roller bearing of the brake via a coupling.

The torque motor can generate a designated torque that can be adjusted with an accuracy of 1 Nm. When the designated torque exceeds the locking capacity of the multi-layer brake, the torque motor will overcome the brake's locking torque and cause an angular displacement of the shaft. Otherwise, the torque motor will be stalled by the multi-layer brake.

An encoder is connected to the shaft serially to measure the angular displacement as shown in Fig. 8. The resolution of the encoder is 4096 counts per revolute (0.088° accuracy). An Arduino-Uno board was used to collect the readings from the

encoder. The Arduino-Uno board also controlled the test rig for sequenced test actions, such as issuing running and stopping commands for the torque motor, actuating and releasing the multi-layer brake, etc.

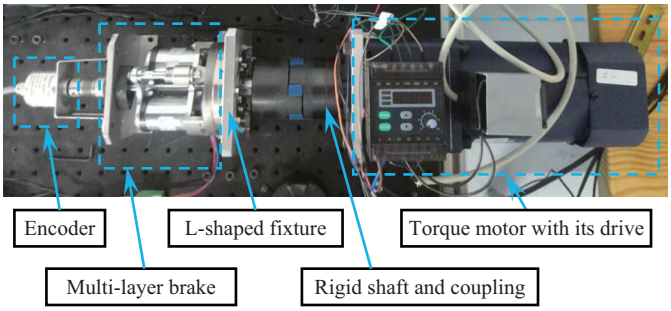

Figure 8. Test rig for the multi-layer brakes

The lifespan of the proposed multi-layer brake was tested through 10,000 testing cycles. The test cycle as shown in Fig. 9 consists of i) a clockwise rotating phase, ii) a clockwise lock-n-load phase, iii) a counter-clockwise rotating phase, and iv) a counter-clockwise lock-n-load phase.

In each lock-n-load phase, a torque that is equal to the rated locking capacity was exerted on the shaft that was connected to the multi-layer brake, for two seconds. The cycle would be stopped if the brake was overcome by the torque motor.

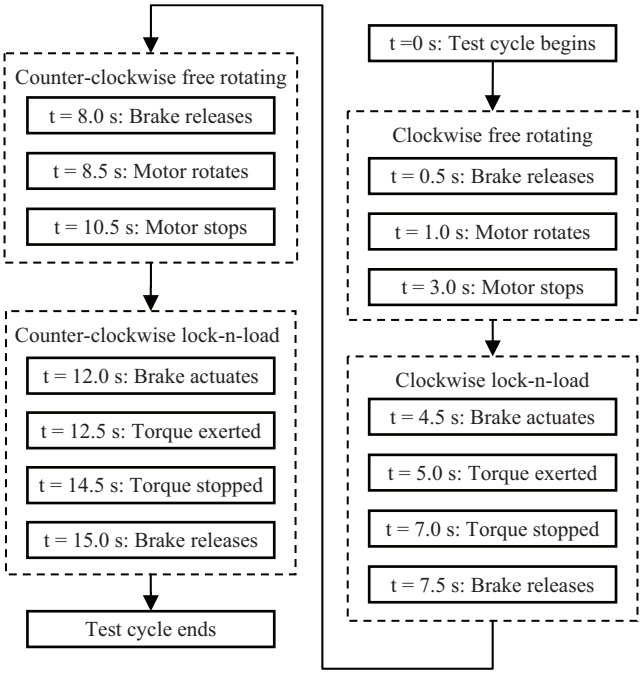

Figure 9. Sequence of a lifespan test cycle

The angular displacement of the shaft for the medium multi-layer brake under the 70-Nm torque within a test cycle is plotted in Fig10. From the inset of Fig. 10, it can be seen that the shaft continues to rotate for about 0.15° when the torque was exerted, due to the finite stiffness of the brake. When the torque was removed, the brake rotated back to the original locking position, indicating the reliability of the locking.

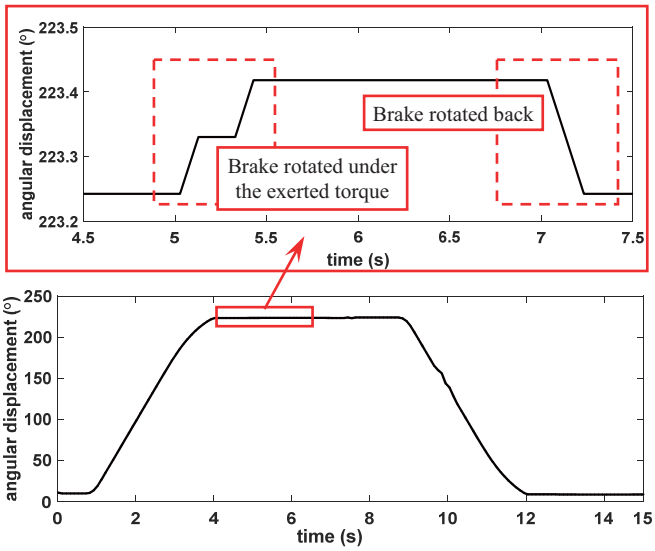

Figure 10. Plot of the angular displacement of the brake

During all the lifespan testing cycles, the angular displacements in both directions were recorded for the large, the medium and the small brakes. A portion of the testing results of the medium brake is plotted in Fig. 11. The maximal angular displacements occurred when the rated torque was exerted, while small residue angular displacements existed when the torque was removed.

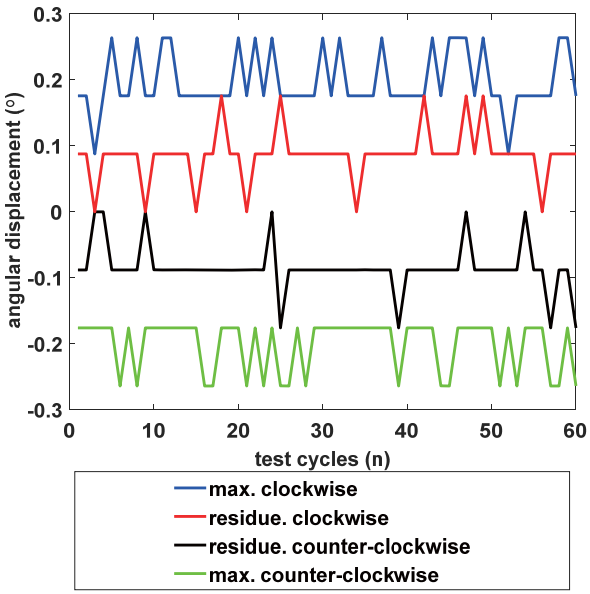

Figure 11. Lifespan testing results of the medim multi-layer brake

The average angular displacements for the large, the medium and the small multi-layer brakes under the rated locking torques are listed in Table II. They are all well below the design goal of 0.5°.

The rotary friction when the brakes were released was tested using a torque gauge. The results are listed in the 5th row of Table II. They are all below 1% of the rated locking capabilities of these brakes. The design goals are also reached.

Next, the maximal locking capacities of these brakes were examined using the torque motor by increasing the output torques gradually. The locking was considered successful if the maximal angular displacement is smaller than 0.5° (as specified in the design goals) after the torque was exerted. The maximal locking capabilities before the lifespan test are listed in the 6th row of Table II.

It is interesting to note that the maximal locking capacities of the brakes after the 10,000-cycle lifespan test are larger than those before the lifespan test. A possible explanation is that the surfaces of the friction disks become abrasive during the lifespan test, leading to an increase in the friction coefficient.

TABLE II. TEST RESULTS OF THE MULTI-LAYER BRAKE

Test Results	Multi-layer brake		
	Large	***Medium***	***Small***
Lifespan testing cycles (times)	10,000	10,000	10,000
Rated locking capacity (Nm)	90	70	40
Average angular displacement (degree)	0.065	0.163	0.204
Released rotary friction (Nm)	0.470	0.141	0.279
Maximal locking capacity (Nm) (Before the lifespan test)	97	74	45
Maximal locking capacity (Nm) (After the lifespan test)	110	98	68

V. CONCLUSIONS AND FUTURE WORKS

Inspired by the layered jamming principle, the paper presents the designs, constructions, and preliminary experimentation of three multi-layer brakes to be applied in a lockable stand for a continuum surgical robotic system, aiming at achieving high locking capability, design compactness, light weight, rapid actuation, and reliable operation.

The brake utilizes a multi-layer structure for amplified locking capability, integrates a cross-roller bearing for design compactness and modularity, and uses electromagnets for rapid actuation. Preliminary experimentation showed that the design goals have all been properly reached.

Immediate future works include investigating possible failure modes of the multi-layer brakes. What's more, their integration in the lockable stands is expected to evaluate the usability of the multi-layer brakes for the continuum surgical robotic system.

REFERENCES

[1] A. Cuschieri, "Laparoscopic Surgery: Current Status, Issues and Future Developments," *The Surgeon,* vol. 3, No.3, pp. 125-138, June 2005.

[2] R. D. Howe and Y. Matsuoka, "Robotics for Surgery," *Annual Review of Biomedical Engineering,* vol. 1, pp. 211-420, Aug 1999.

[3] R. H. Taylor and D. Stoianovici, "Medical Robotics in Computer-Integrated Surgery," *IEEE Transactions on Robotics and Automation,* vol. 19, No.3, pp. 765-781, 2003.

[4] C. Bergeles and G.-Z. Yang, "From Passive Tool Holders to Microsurgeons: Safer, Smaller, Smarter Surgical Robots," *IEEE Transactions on Biomedical Engineering,* vol. 61, No.5, pp. 1565-1576, May 2014.

[5] M. C. Cavusoglu, M. Cohn, F. Tendick, and S. Sastry, "A Laparoscopic Telesurgical Workstation," *IEEE Transactions on Robotics and Automation,* vol. 15, No.4, pp. 728-739, 1999.

[6] G. S. Guthart and J. K. Salisbury, "The Intuitive™ Telesurgery System: Overview and Application," in *IEEE International Conference on Robotics and Automation (ICRA)*, San Francisco, CA, 2000, pp. 618-621.

[7] P. Berkelman and J. Ma, "A Compact Modular Teleoperated Robotic System for Laparoscopic Surgery," *The International Journal of Robotics Research,* vol. 28, No.9, pp. 1198-1215, 2009.

[8] B. Hannaford, J. Rosen, D. W. Friedman, H. King, P. Roan, L. Cheng, D. Glozman, J. Ma, S. N. Kosari, and L. White, "Raven-II: An Open Platform for Surgical Robotics Research," *IEEE Transactions on Biomedical Engineering,* vol. 60, No.4, pp. 954-959, April 2013.

[9] C.-H. Kuo, J. S. Dai, and P. Dasgupta, "Kinematic Design Considerations for Minimally Invasive Surgical Robots: an Overview," *The International Journal of Medical Robotics and Computer Assisted Surgery,* vol. 8, No.2, pp. 127-145, June 2012.

[10] H. Azimian, R. V. Patel, and M. D. Naish, "On Constrained Manipulation in Robotics-Assisted Minimally Invasive Surgery," in *IEEE / RAS-EMBS International Conference on Biomedical Robotics and Biomechatronics (BIOROB)*, Tokyo, Japan, 2010, pp. 650-655.

[11] C.-H. Kuo and J. S. Dai, "Kinematics of a Fully-Decoupled Remote Center-of-Motion Parallel Manipulator for Minimally Invasive Surgery," *Journal of Medical Devices,* vol. 6, No.2, p. 021008, May 2012.

[12] K. Xu, R. E. Goldman, J. Ding, P. K. Allen, D. L. Fowler, and N. Simaan, "System Design of an Insertable Robotic Effector Platform for Single Port Access (SPA) Surgery," in *IEEE/RSJ International Conference on Intelligent Robots and Systems (IROS)*, St. Louis, MO, USA, 2009, pp. 5546-5552.

[13] J. Ding, R. E. Goldman, K. Xu, P. K. Allen, D. L. Fowler, and N. Simaan, "Design and Coordination Kinematics of an Insertable Robotic Effectors Platform for Single-Port Access Surgery," *IEEE/ASME Transactions on Mechatronics,* vol. 18, No.5, pp. 1612-1624, Oct 2013.

[14] K. Xu, J. Zhao, and M. Fu, "Development of the SJTU Unfoldable Robotic System (SURS) for Single Port Laparoscopy," *IEEE/ASME Transactions on Mechatronics,* vol. 20, No.5, pp. 2133-2145, Oct 2015.

[15] J. S. Brar and R. K. Bansal, *A TextBook of Theory of Machines*, 4th Revised edition ed.: Laxmi Publications, 2010.

[16] J. M. D. Coey, "Permanent Magnet Applications," *Journal of Magnetism and Magnetic Materials,* vol. 248, No.3, pp. 441-456, Aug 2002.

[17] Y.-J. Kim, S. Cheng, S. Kim, and K. Iagnemma, "A Novel Layer Jamming Mechanism With Tunable Stiffness Capability for Minimally Invasive Surgery," *IEEE Transactions on Robotics,* vol. 29, No.4, pp. 1031-1042, Aug 2013.

[18] J. Ou, L. Yao, D. Tauber, J. Steimle, R. Niiyama, and H. Ishii, "jamSheets: Thin Interfaces with Tunable Stiffness Enabled by Layer Jamming," in *International Conference on Tangible, Embedded and Embodied Interaction (TEI)*, New York, NY, USA, 2014, pp. 65-72.

[19] R. J. Farris and M. Goldfarb, "Design of a Multi-Disc Electromechanical Modulated Dissipator," in *IEEE International Conference on Robotics and Automation (ICRA)*, Anchorage, Alaska, USA, 2010, pp. 2189-2196.